

Structural and dielectric properties of superparamagnetic iron oxide nanoparticles (SPIONs) stabilized by sugar solutions

D. SIVA KUMAR^{1,3}, K. CHANDRA BABU NAIDU², M. MOHAMED RAFI³, K. PREM NAZEER^{3,*},
A. AYISHA BEGAM⁴, G. RAMESH KUMAR⁵

¹Department of Physics, Sree Krishna College of Engineering, Unai, Anaicut-632 101, Tamilnadu, India

²Department of Physics, Material Science Laboratory, S.K.University, Anantapur-515 003, A.P., India

³PG & Research Department of Physics, Islamiah College, Vaniyambadi-635 752, Tamilnadu, India

⁴Department of Physics, Avinashilingam Institute for Home Science and Higher Education, Coimbatore-641 043, Tamilnadu, India

⁵Department of Physics, University College of Engineering-Arni, 632 326, Tamilnadu, India

Superparamagnetic iron oxide nanoparticles (SPIONs) have been synthesized using co-precipitation method. Their microstructure and dielectric properties were studied. The sugar solutions like glucose, fructose and sucrose were used as stabilizers to control the size of the SPIONs. The crystal structure and grain size of the particles were determined by X-ray diffraction. The magnetic studies of the samples were carried out using the vibrating sample magnetometer and their surface morphology was studied by HRTEM, FE-SEM and zeta potential. The dielectric properties of glucose-SPIONs (GF), fructose-SPIONs (FF) and sucrose-SPIONs (SF) were investigated in the frequency range of 10 Hz to 5 MHz at selected temperatures. The FF showed a high dielectric constant of 62 at 1 MHz and the dielectric properties of SPIONs were found to have been significantly improved, especially in the low frequency regime according to the Maxwell-Wagner interfacial polarization. The AC conductivity measurements revealed that the electrical conduction depends on both frequency and temperature. Impedance analysis was carried out using Cole-Cole plot and the conduction mechanism of the studied compounds was explained. R and C values were further calculated using RC-circuit.

Keywords: *SPIONs; sugar solutions; XRD; VSM; FE-SEM; dielectric properties*

1. Introduction

Biopolymer chitosan is known for its excellent film forming ability, high mechanical strength, biocompatibility, non-toxicity, high permeability towards water, susceptibility to chemical modifications, cost-effectiveness, etc. More than a few attempts have been undertaken to increase the activity of chitosan and, in particular, its biocompatibility by structural modification through the fabrication of nanocomposites with metal oxide nanoparticles [1]. Amongst all iron oxide nanoparticles, magnetite (Fe_3O_4) represents the most remarkable properties due to its unique structure, i.e.

the presence of iron cations in two valence states Fe^{2+} and Fe^{3+} on tetrahedral and octahedral sites with an inverse cubic spinel structure [2]. The electrons can hop between Fe^{2+} and Fe^{3+} ions creating octahedral sites at room temperature forming magnetite, an important class of half-metallic materials [3]. However, aggregation of Fe_3O_4 nanoparticles, due to high surface area of magnetic dipole interaction between nanoparticles, has limited their applications. This problem can be solved by dispersing Fe_3O_4 nanoparticles in a biopolymer matrix [4, 5]. The biopolymer chitosan is a poly-amino-saccharide produced by de-acetylation of natural chitin which could be extracted from the shells of crabs and shrimps. It shows excellent biocompatibility, high mechanical strength

*E-mail: sivadhananjayan@gmail.com

and susceptibility to chemical modification due to the presence of reactive hydroxyl and amino functional groups [5]. The magnetite (Fe_3O_4) shows high M_s values due to antiferromagnetic ordering across tetrahedral (Fe^{3+}) and octahedral (Fe^{2+} and Fe^{3+}) sublattices. In the past decade, Fe_3O_4 nanoparticles of different morphologies, chemical substitutions and surface coatings were used to learn quite a lot of the applications such as magnetic resonance imaging (MRI), contrast agents [6, 7], drug delivery [8], tissue repair [9], in-vivo applications such as detoxification of biological fluids, immunoassay, cell variation and hyperthermia [10] and microwave applications at high and low frequencies [11].

In the present study, the SPIONs stabilized by sugar solutions have been prepared by coprecipitation method. They were systematically investigated by X-ray diffraction for crystallite size and structure. The morphological characteristics of the prepared nanoparticles were studied by transmission and scanning electron microscope. Further, the magnetic properties were studied using vibrating sample magnetometer (VSM) and zeta potential. The dielectric properties were studied as a function of frequency at different temperatures.

2. Experimental

Glucose, fructose, sucrose and the reagents including $\text{FeCl}_3 \cdot 6\text{H}_2\text{O}$, $\text{FeSO}_4 \cdot 7\text{H}_2\text{O}$, $\text{NH}_3\text{H}_2\text{O}$ and ethanol were procured from Fisher Scientific, India. All the chemicals were used in as-received state without any further purification.

2.1. Synthesis of glucose- Fe_3O_4 (GF), fructose- Fe_3O_4 (FF) and sucrose- Fe_3O_4 (SF)

Stabilizers such as glucose, fructose and sucrose of 1.2 g each were added to 200 mL distilled water. The blend was heated at 90 °C for about 10 min at constant stirring for dissolution of the sugar solution. The solution was consequently cooled to the room temperature, afterwards $\text{FeCl}_3 \cdot 6\text{H}_2\text{O}$ (1.49 g) and $\text{FeSO}_4 \cdot 7\text{H}_2\text{O}$ (0.765 g) were added into the solution, which was then

heated at 60 °C under nitrogen atmosphere. Then the pH value of the solution was adjusted to around 11 by dropwise addition of ammonia hydroxide solution for all stabilizers chosen for this study. The resultant solution (8 mol/L) was held at 60 °C for 4 hours and the suspension was then centrifuged at 10000 rpm for 10 minutes. The settled sugar solution stabilized by SPIONs was washed three times using distilled water to remove byproducts and excess sugar solution. The obtained hybrids were dried in an oven at 100 °C for 3 h and labeled as GF, FF and SF, respectively.

2.2. Characterization

The crystal structure of the samples was identified by X-ray diffraction (XRD) using a Bruker Model: D8 advance diffractometer with $\text{CuK}\alpha$ radiation (1.5406 Å), operating at 40 kV and 30 mA. The surface morphology of the synthesized samples was examined by high resolution transmission electron microscope (HRTEM, JEOL JEM 2100) and field emission scanning electron microscope (FE-SEM, JEOL-JSM-6390 LV). The magnetic properties of the samples were studied by vibrating sample magnetometers (VSM, Lakeshore 7410) at room temperature. The zeta potential stability of nanoparticles was measured on Malvern Zetasizer and the dielectric properties, such as dielectric constant ϵ_r and dielectric loss $\tan\delta$ were studied with the aid of HIOKI 3532-50 LCR Hi TESTER. For the dielectric measurements, the pellets were sputtered with silver paste on both sides without contacting the edges and were kept on platinum electrodes of an LCR controller in temperature ranging from 350 K to 400 K, operated at the frequencies from 10 KHz to 5 MHz at a heating rate of 5 °C/min.

3. Results and discussion

3.1. X-ray diffraction studies

The crystalline structure of GF, FF and SF was examined by X-ray diffraction study and has been depicted in Fig. 1. Five characteristic peaks can be indexed as the cubic structure Fe_3O_4 , which is in accordance with the reported data (JCPDS

Card No. 82-1533). The peaks with 2θ values of 30.38° , 35.64° , 43.33° , 57.47° , 62.89° correspond to the crystal planes (2 2 0), (3 1 1), (4 0 0), (3 3 3), (4 4 0) of crystalline Fe_3O_4 , respectively. The crystallite diameter (D) of the nanoparticles was estimated using Debye-Scherrer formula [12]:

$$D = k\lambda / \beta \cos \theta \quad (1)$$

where k is crystallite geometry dependent constant and is 0.94 for spherical crystallites, λ is the wavelength of X-ray radiation used, β is full-width at half-maximum of the peak profile in radians at 2θ angle, 2θ is the angle of diffraction with respect to lattice planes. The peak width obviously was broadened in the curve FF as compared with the curves SF and GF. The average crystallite sizes were calculated using equation 1 which gave 3.38 nm, 4.82 nm and 5.23 nm for GF, FF and SF from the maximum intense peak of (3 1 1), respectively.

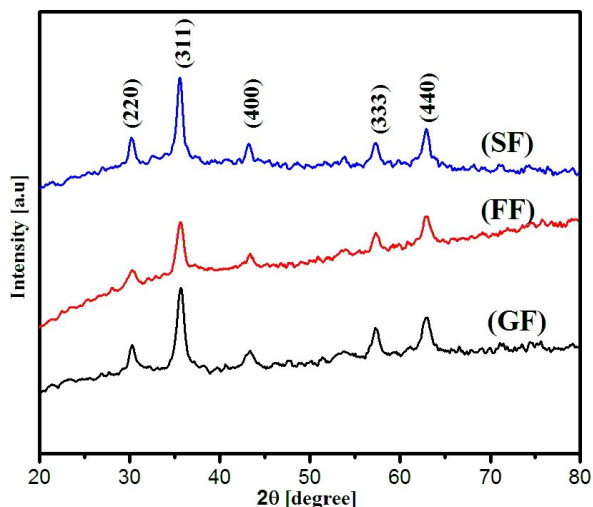


Fig. 1. XRD patterns of GF, FF and SF.

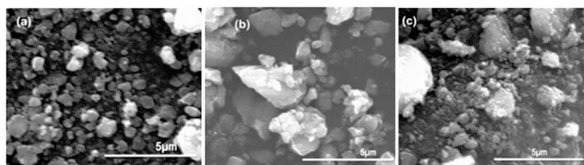


Fig. 2. FE-SEM images of (a) GF, (b) FF, (c) SF.

The field emission scanning electron microscope (FE-SEM) images of GF, FF and SF are

shown in Fig. 2. It is found that all the samples have well defined grains. An even distribution of the magnetite nanoparticles can be observed in all the images. In the SEM images, few dislocations and grains along with grain boundaries have been observed [13]. The average grain sizes of FF (648 nm), SF (520 nm) and GF (469 nm) have been found using the linear intercept method. In addition, the agglomeration of nanoparticles is observed for all the samples. This agglomeration phenomenon is due to the magnetic interactions among the nanoparticles. Fig. 3 shows the HRTEM images of GF, FF and SF nanoparticles. The average particle size of the synthesized NPs is 7.5 nm, 7.2 nm and 10.46 nm. The magnetic interaction between the nanoparticles is responsible for the agglomeration in HRTEM photographs. The overall analysis of morphology proves that the grain size of the present samples observed in FE-SEM micrographs is greater than the particle size obtained from the HRTEM images. This difference may be attributed to the agglomeration of fine powder.

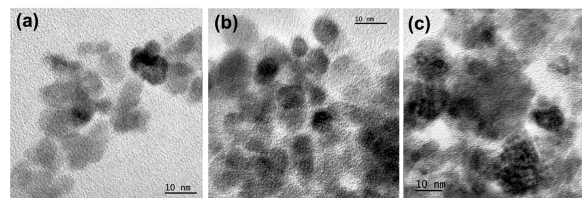


Fig. 3. HRTEM images of (a) GF, (b) FF, (c) SF.

3.2. Magnetic properties analysis

The magnetic properties of the nanoparticles at the room temperature were studied using a vibrating sample magnetometer and the magnetization values of the samples were systematically recorded as a function of applied magnetic field to an extent of 15000 Gauss. The observed magnetization curves of GF, FF and SF are shown in Fig. 4. The hysteresis loop shows no remanence and coercivity upon reducing the field towards the opposite direction. The magnetization curves demonstrate a typical superparamagnetic behavior which shows high susceptibility with saturated magnetization M_s at low field strength and zero coercivity and remanence.

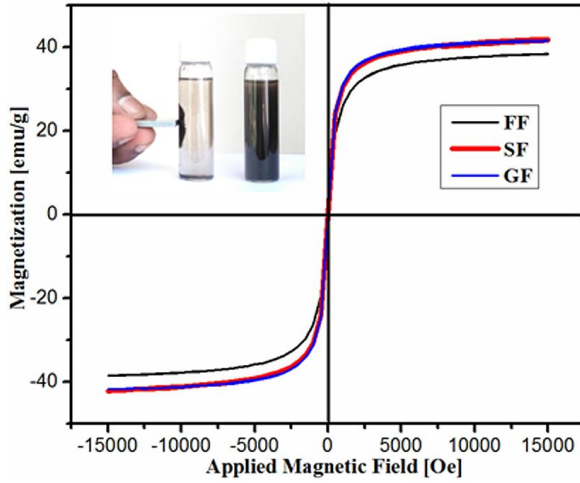


Fig. 4. Magnetization curves of GF, FF and SF.

The magnetic parameters of GF, FF and SF are shown in Table 1. M_s values 41.69 emu/g, 38.43 emu/g and 42 emu/g have been estimated for GF, FF and SF samples, respectively which could be attributed to the presence of sugar solutions on the stabilized of nanospheres. Magnetic nanoparticles intrinsically show reduced magnetization due to disordered magnetic spins at surface of the nanoparticles, though the particles are of crystalline nature. The percentage of disordered spins enhances with reduction of particle size due to the increase of surface area-to-volume ratio [14].

3.3. Dielectric properties

Dielectric measurements were carried out at room temperature over a wide frequency range from 100 Hz up to 5 MHz. The dielectric constant ϵ' and loss tangent $\tan\delta$ were calculated using the formula:

$$\epsilon' = cd/\epsilon_0 A \quad (2)$$

$$\tan\delta = \epsilon''/\epsilon' \quad (3)$$

where c is the capacitance, d the thickness of the sample, A the cross-section area, ϵ_0 the free space permittivity (8.854×10^{-12} F/m). The results are collected in Table 2 at selected frequencies and room temperature.

3.3.1. Frequency dependence

The frequency dependences of dielectric constant ϵ_r and loss tangent $\tan\delta$ as a function of frequency in the range of 100 Hz to 5 MHz are shown in Fig. 5. The behavior of dielectric constant and loss tangent depends on the relation of AC conductivity versus frequency. It is observed that for the GF and SF, the highest conductivity results in the highest ϵ_r and $\tan\delta$ values and vice-versa. As a normal dielectric behavior of spinel SPIONs, ϵ_r is decreasing with frequency for all the SF, FF and GF samples. The Koop phenomenon (double-layer dielectric model) gives a theoretical illustration for attaining high relative permittivity and loss at low frequencies [15]. It has been confirmed that at lower frequency, the dipoles within the system can reorient themselves to respond to the applied electric field. On the other hand, at higher frequency, the decrease of dielectric constant values is attributed to the blocking of molecules in the applied field direction, which could be explained by the difficulty of dipoles reorientation in this frequency range [16]. In accordance with this model, spinel ferrites of crystalline nature contain a couple of layers called grains and grain boundaries where the grains are low-resistive while grain boundaries are high-resistive. These grain boundaries are more active at low frequencies and offer quick response to the applied alternating field frequency resulting in high polarization. The dielectric constant increases with the increasing temperature and this increase may be due to the thermal energy supplied to the material that is sufficient enough to the free localized dipoles which align themselves in the direction of applied field [17]. The dielectric parameters are listed in Table 2. It can be understood from the table that the Curie transition temperature of iron oxide is increased with varying the coated compound (GF to SF). In respect of dielectric constant, an appreciable increase is observed for the FF material. On the other hand, high loss tangent is observed for SF at 1 MHz. It is well known that the loss is directly proportional to AC conductivity and thus, in turn, the SF shows high conductivity. The dielectric relative loss factor is also calculated from $\tan\delta/\epsilon_r$. This is a measure of purity of a sample. It

Table 1. Magnetic parameters obtained from VSM analysis.

Sample code	Saturation magnetization M_s [emu/g]	Coercivity H_c [Oe]	Remanent magnetization M_r [emu/g]	Remanence ratio (M_r/M_s)
GF	41.69	0.55	0.0004	0
FF	38.43	4.42	0.004	0
SF	42	9.13	0.0098	0

implies that the relative loss factor should be as low as possible for high purity material.

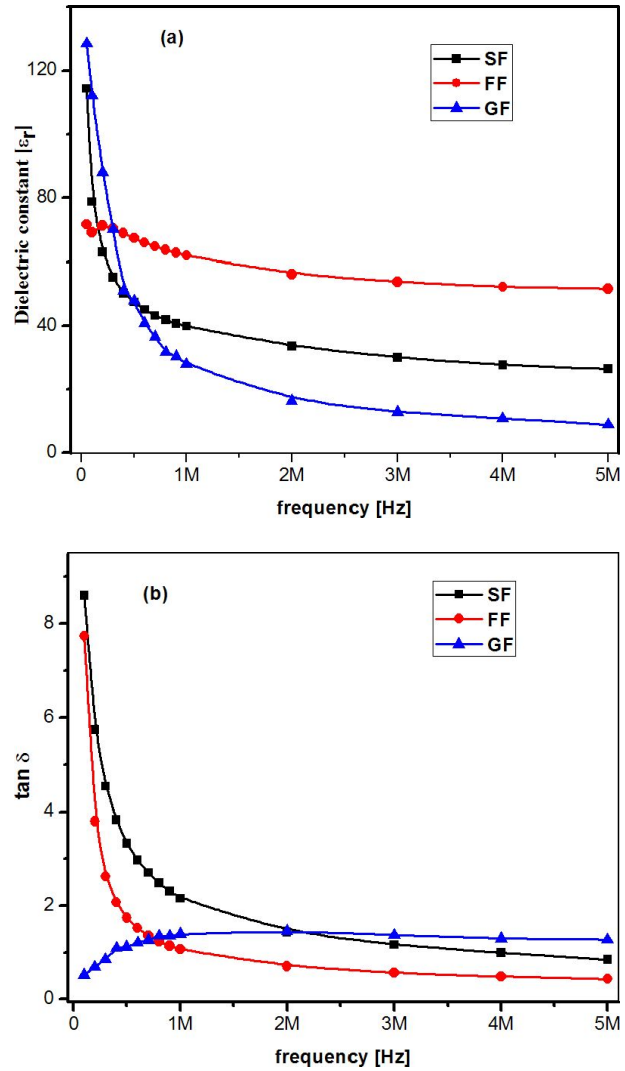
Table 2. Data on of electrical properties of GF, FF and SF.

X	GF	FF	SF
T_c	323 K	338 K	343 K
ϵ_r [1 MHz]	27.9	61.94	39.68
$\tan\delta$ [1 MHz]	1.39	1.06	2.15
$\tan\delta/\epsilon_r$	0.05	0.0171	0.0542
σ_{dc} [S/cm]	4.17E-11	5.25E-11	2.45E-10
exponent (n)	0.94	0.49	0.411

3.3.2. Temperature dependence

The temperature dependences of relative permittivity ϵ_r and loss tangent $\tan\delta$ are shown at 1 MHz frequency. Fig. 6 reveal that ϵ_r as well as $\tan\delta$ are increasing with rising temperature for all the GF, SF and FF samples. This kind of behavior is commonly observed in magnetic semiconductor SPIONs.

The drift velocity of thermally activated charge carriers increases with temperature. Hence, the electron exchange between Fe^{3+} - Fe^{2+} ions on the both sites is increased [18]. The local displacement of the thermally activated carriers in response to the alternating field frequency causes that all the carriers reach the grain boundary interface and tend to increase polarization. The relaxation peaks in loss tangent plots are observed in the temperature range of 323 K to 365 K. These relaxations are mainly caused by the maximum thermal activation of hopping rate of charge carriers. Thus, the polarization increases and the resistivity decreases, resulting in an enhancement of $\tan\delta$ [19]. The results are shown in Table 2. ϵ_r and $\tan\delta$ increase with temperature. At room temperature, the sample shows very high

Fig. 5. Frequency dependence of (a) dielectric constant ϵ_r and (b) loss tangent $\tan\delta$.

loss. GF = 1.39, FF = 1.06 and SF = 2.15 are obtained at 1 MHz field frequency. This kind of compounds with high loss is normally expected for absorber applications at high frequency [20].

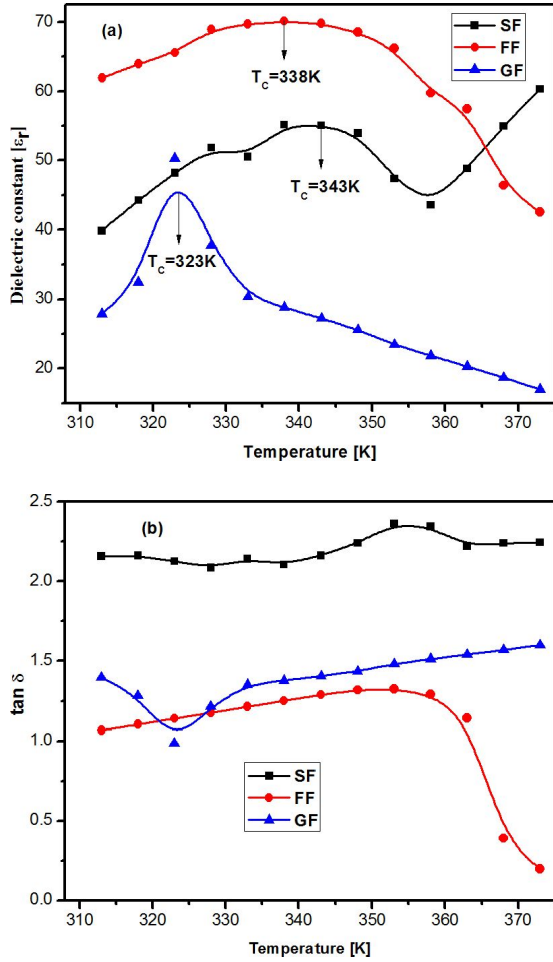


Fig. 6. Temperature dependence of (a) dielectric constant ϵ_r and (b) loss tangent $\tan \delta$.

3.3.3. Conductivity studies

The variation of AC conductivity as a function of frequency at room temperature is illustrated in Fig. 7. It is obvious from $\log \sigma$ versus $\log \omega$ plots that the total AC conductivity is composed of two frequency terms [21]. Jonscher power law [22] can successfully explain the analyzed variation of AC conductivity with frequency. The frequency independent term (linear portion) is clearly determined in $\log \sigma$ versus $\log \omega$ plots. A linear portion is extrapolated towards the $\log \sigma$ axis. The second term is frequency dependent and increases with frequency due to localized charge carriers. This is governed by the power law:

$$\sigma_{ac}(\omega) = A\omega^n \quad (4)$$

where $\omega = 2\pi f$, A is the arbitrary constant and the exponent n has values between 0 and 1 with no dimension. Both entities are temperature dependent [23]. The small values of AC conductivity σ_{ac} at lower frequencies and its increasing trend at the higher frequencies can be elucidated by Maxwell-Wagner theory [24]. This increase in σ_{ac} may be normally due to the grain and grain boundary effect that is caused by the inhomogeneous nature of dielectric medium [25]. The σ_{ac} values of magnetite nanoparticles stabilized by various sugar molecules are reported in Table 2. The exponent value n mentioned in the relation 4 gives the ratio of the back-hop rate to the site relaxation rate. If the exponents are less than 1, the polaron hopping is slower than the site relaxation. If the hopping of polarons is larger than the site relaxation, the exponents are greater than one. In Fig. 7, the exponent values of GF, FF and SF are $n = 0.94, 0.49$ and 0.411 , respectively. As shown in Fig. 7 the DC conductivity values have been calculated and found to be varying between 2.45×10^{-10} S/cm and 5.24×10^{-11} S/cm.

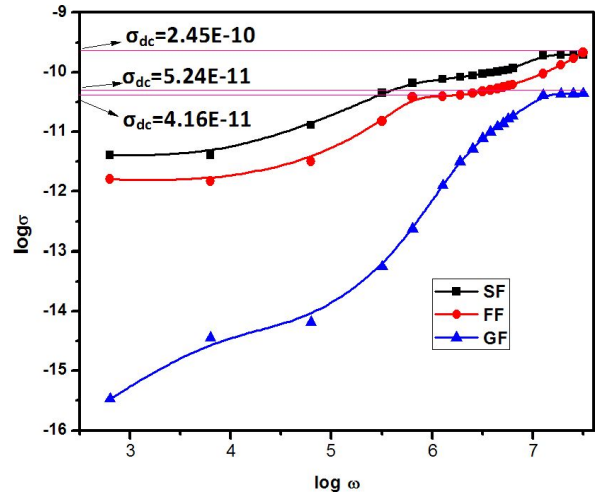


Fig. 7. $\log \sigma$ versus $\log \omega$ plot of AC electrical conductivity of GF, FF and SF.

The AC conductivity σ_{ac} is calculated using the relation:

$$\sigma_{ac} = \epsilon_r \epsilon_0 \tan \delta \quad (5)$$

where ω is the angular frequency, ϵ_r is the relative dielectric constant, ϵ_0 is the permittivity of free

space and $\tan\delta$ is the tangent loss. The AC conductivity versus temperature plots (Fig. 8) show that the conductivity is increasing with temperature up to T_c and further starts decreasing to smaller values. Thus, it obeys the Arrhenius relation. The $\ln\sigma_{ac}$ versus $1/T$ plots show two slopes in two regions. It is proposed that on passing through the Curie point T_c a change in the slope of the straight line occurs due to the change in exchange interaction between outer and inner electrons at T_c . In the present investigation, the change of the slope may be expected due to the change in conduction mechanism illustrated by the calculated activation energies within the low and high temperature regions. In the high temperature regime, the steady state rise in conductivity is ascribed to polaron hopping and the thermal expansion of the lattice is accompanied by lattice dislocations and creates polarons. In case of low temperature region, the electrical conductivity is due to thermally activated electrons. The activation energies E_a are evaluated from the $\ln\sigma_{ac}$ versus temperature plots using Arrhenius equation 6 and equation 7:

$$\sigma_{ac} = \sigma_0 \exp(-E_a/kT) \quad (6)$$

$$E_a = \text{slope} \times k_b \times 10^3 \text{ eV} \quad (7)$$

where the slope is $\ln\sigma_{ac}$ versus $1000/T$, k is Boltzmann constant (8.6×10^{-5} eV) and σ_0 is the pre-exponential factor. The results show that the AC activation energies of all materials in low temperature region (E_1) are greater than in the high temperature region (E_2). It may be related to the disordered state in high temperature region with respect to the ordered state in low temperature region as reported by Naidu et al. [26].

3.3.4. Impedance properties

Impedance spectroscopy is used to study transport properties of GF, FF and SF at different applied electric field frequencies within a wide temperature range. Impedance is a complex quantity and its real part gives a series resistance while the imaginary part represents reactance of the compound. In general, complex impedance spectroscopy is a well-known technique to

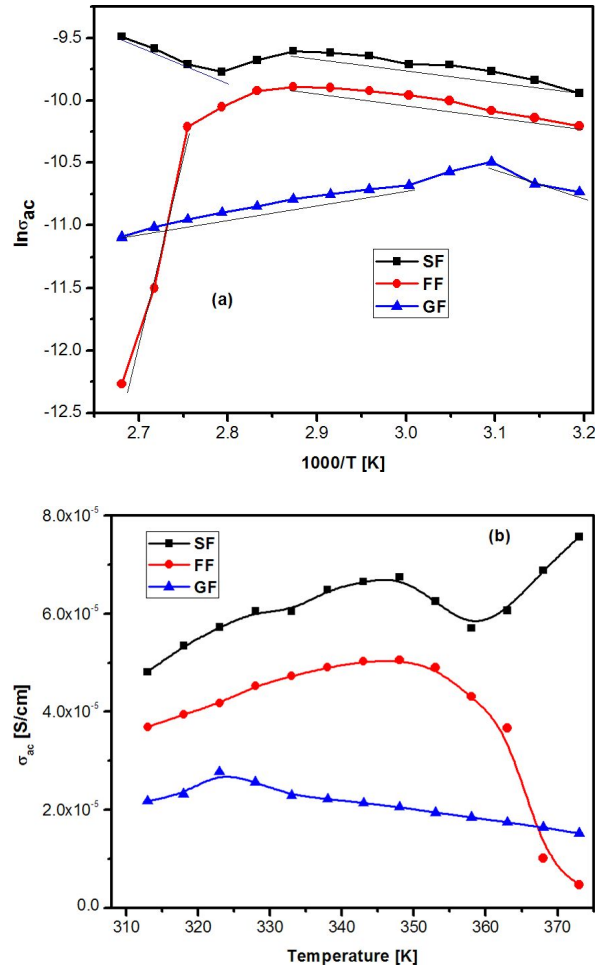


Fig. 8. (a) $\ln\sigma_{ac}$ versus $10^3/T$ plots, (b) σ_{ac} versus temperature plots.

probe microstructure and electrical conduction mechanism of polycrystalline materials [27]. It also enables to resolve grain (bulk) and grain boundary effects in conductivity studies including relaxation. Complex impedance has a basic formalism: $Z^* = Z' - jZ''$, where Z' is the real part and Z'' is imaginary part. Fig. 9 depicts the Z' versus Z'' plots (Nyquist plots) at the selected temperatures (313 K to 380 K). It is evident from the Cole-Cole plots that single semicircular arcs observed for all the temperatures obviously represent the two-layer model of conduction mechanism, i.e. grain and grain boundaries are contributing in conduction mechanism [28]. This confirms that the synthesized ferrites are of magnetic semiconductors. The centers

Table 3. Activation energy of GF, FF and SF.

Sample code	Activation energy [eV]	
	E_1	E_2
GF	0.204	0.103
FF	2.629	0.077
SF	0.276	0.076

of semicircular arcs lying above Z' -axis (real axis) reveal Debye-type relaxations [29–31]. The large semicircular arc at the higher frequencies and the small semicircular arcs at the lower frequencies are associated to grain and grain-boundary effects, respectively. The corresponding resistances (R_g and R_{gb}) and capacitances (C_g and C_{gb}) are evaluated from the intersecting points of arcs at the real axis using Z-view software. These resistances are found to be decreasing with increasing temperature and reveal the increase of DC electrical conductivity. Furthermore, the relaxation time τ has been calculated as $\tau = RC$. It is noticed that τ is decreasing with the increase of temperature. This, in turn, reveals that τ is a temperature dependent parameter [32]. The σ_{dc} is calculated using the relation:

$$\sigma_{dc} = t/RA \quad (8)$$

where t is the sample thickness, R is the bulk or grain boundary resistance and A is the area of the sample. According to Arrhenius law:

$$\sigma_{dc} = \sigma_0 \exp(-E_a/k_bT) \quad (9)$$

where the symbols have their usual meaning. In σ versus $10^3/T$ plots have been drawn to find the activation energies as shown in Fig. 10. The results show that the activation energy is decreasing with the increase in SF, GF and FF content. The corresponding activation energies (E_a) are tabulated in Table 3; the results are estimated to be GF = 0.210 eV, SF = 0.115 eV and FF = 0.032 eV, respectively.

3.3.5. Role of sugar solutions on the stability of SPIONs

Chalikian *et al.* [33] and Höchtl *et al.* [34] have reported that the hydration properties of sugar solutions are, in general, a key feature in determining

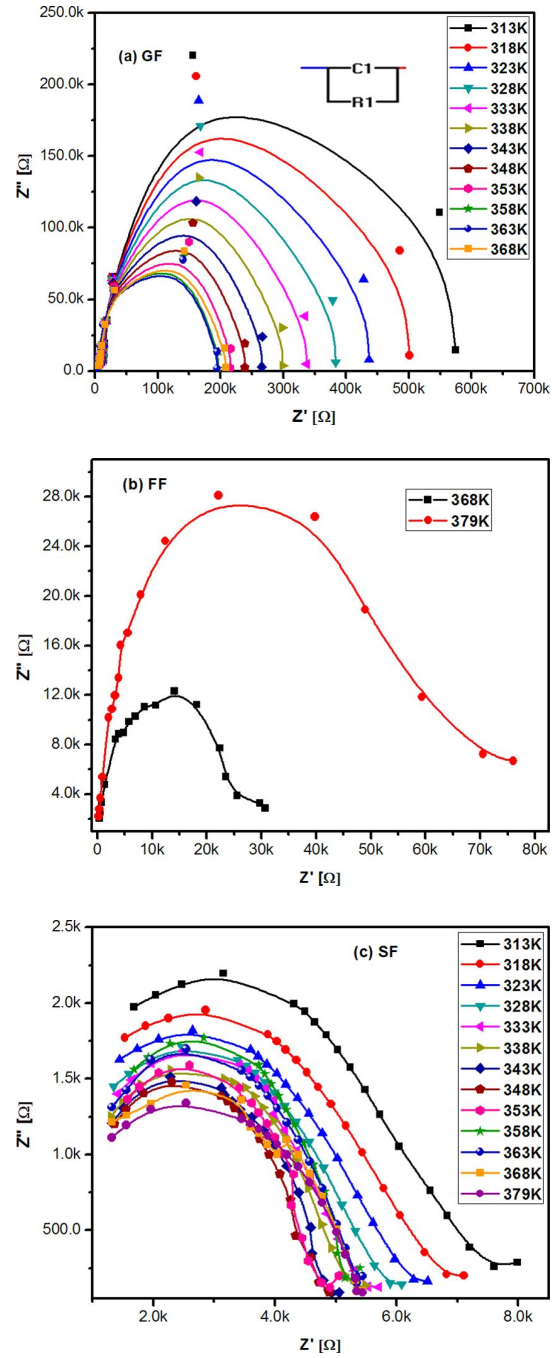


Fig. 9. Z' versus Z'' plots (Nyquist plots) for (a) GF, (b) FF and (c) SF.

their functional as well as the structural properties. Accordingly, the variation in hydration properties of glucose, fructose and sucrose greatly contributes on the stereo conformation of SPIONs when it is stabilized by sugar molecules.

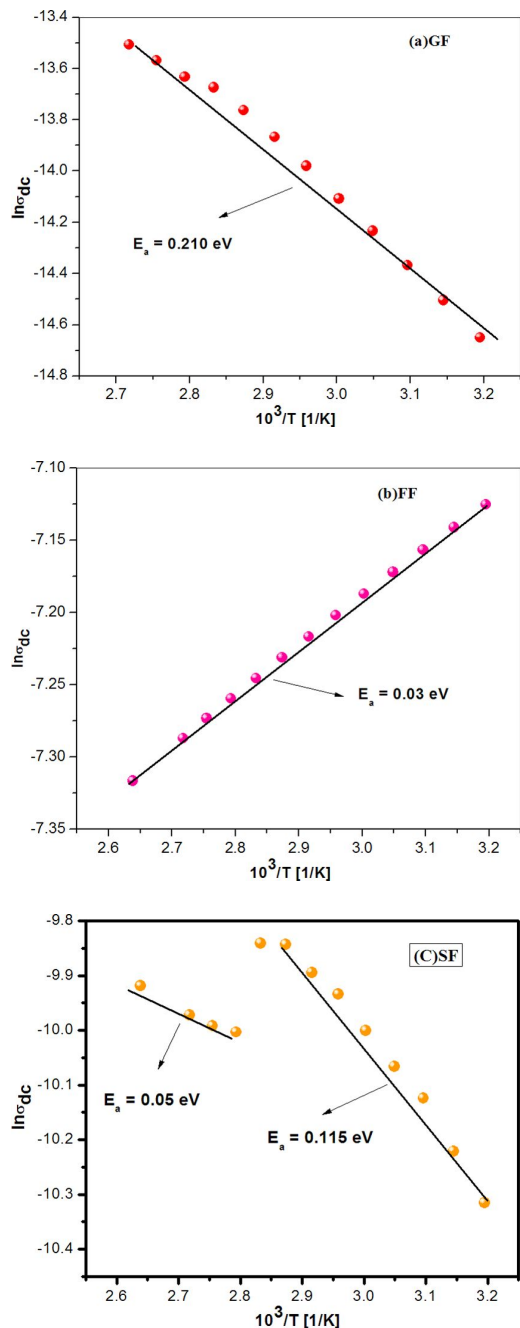


Fig. 10. Arrhenius plots for (a) GF, (b) FF and (c) SF derived from impedance spectra at different temperatures.

Further, it has been reported that the dipole moments of fructose and sucrose are slightly greater than glucose in pure state (Table 4). However, while observing the zeta potential values (obtained from dynamic laser scattering), it can be inferred

that there is an appreciable increase in the stability of colloidal dispersion over fructose and sucrose solutions when SPIONs are stabilized with glucose (Fig. 11).

Jansson et al. [35] reported that hydrated sugar molecules always exhibit a non-Arrhenius temperature dependence of its relaxation time. Consequently, due to α -relaxation process, they have a slower relaxation time. Considering the τ_c values, glucose solution has the slowest value, when comparing with fructose and sucrose. As viscosity is strongly dependent on relaxation time, higher viscosity glucose aided SPIONs is characterized by highest stability. As rightly concluded by Tait et al. [36] and Franks et al. [37], the hydration number gives a fair clue on the conformational behavior of sugar molecules.

Table 4. Comparison of relaxation time, hydration number and zeta potential.

Sample code	Relaxation time (τ_c) [s]	Hydration number	Zeta potential [mV]
GF	5.73×10^{-06}	2.0	25.9
FF	1.62×10^{-07}	1.7	10.6
SF	7.83×10^{-08}	1.5	1.85

4. Conclusions

Iron oxide nanoparticles with superparamagnetic character have been successfully synthesized by co-precipitation method and their magnetite nanoparticles have been subsequently stabilized using sugar solutions of glucose, fructose and sucrose. Powder X-ray diffraction results show that the obtained magnetic particles are nanosized and their unit cell exhibits face-centered cubic structure. Saturation magnetization values of all studied SPIONs stabilized by sugar molecules are in the range of 38.43 emu/g to 42 emu/g. Coercivity of the nanoparticles stabilized by glucose shows the lowest value when compared to other sugar solutions. SPIONs stabilized by fructose have low dielectric relaxation time which is increasing with temperature. It was found that the dielectric constants and dielectric loss values of SPIONs stabilized

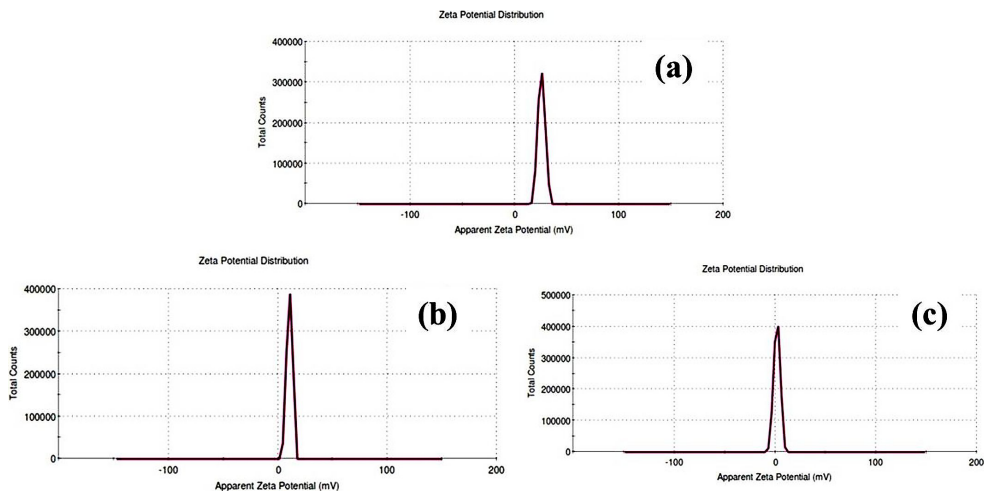


Fig. 11. Zeta potential stability of SPIONs: (a) GF, (b) FF and (c) SF

by sugar solutions are as follows: (i) GF, $\epsilon_r = 27.9$, $\tan\delta = 1.39$; (ii) FF, $\epsilon_r = 61.94$, $\tan\delta = 1.06$ and (iii) SF, $\epsilon_r = 39.68$, $\tan\delta = 2.15$.

The activation energies of GF, FF and SF vary between 0.103 eV and 2.629 eV. It has been suggested that relaxation time, hydration number and kinematic viscosity of sugar solutions, especially glucose, play a significant role in determining the long term stability of magnetite nanoparticles. From the above studies, it can be concluded that SPIONs stabilized by sugar molecules can be used for super capacitors and magnetic recording applications.

Acknowledgements

The authors are thankful to Dr. A. Mohan., Department of Physics, the School of Advanced Sciences, the VIT University, Vellore-632 014, Tamil Nadu, India, for fruitful discussions. One of the authors, Mr. D. Sivakumar, wishes to acknowledge Dr. B. Sathyaseelan & Mr. G. Killivalavan, Department of Physics, the University College of Engineering-Arni, 632 326 Tamilnadu, India, for their timely help and moral support extended to prepare this manuscript.

References

- [1] BHATT A.S., KRISHNA BHAT D., SANTOSH M.S., *J. Phys.-Condens. Mat.*, 405 (2010), 2078.
- [2] RAHMAN O., MOHAPATRA S.C., AHMAD S., *Mater. Chem. Phys.*, 132 (2012), 196.
- [3] OZKAYA T., TOPRAK M.S., BAYKAL A., KAVAS H., AKTAS B., *J. Alloy. Compd.*, 472 (2009), 18.
- [4] KAUSHIK A., KHAN R., SOLANKI P.R., PANDEY P., ALAM J., AHMAD S., MALHOTRA B.D., *Biosen. Bioelectron.*, 24 (2008), 676.
- [5] KAUSHIK A., SOLANKI P.R., ANSARI A.A., MALHOTRA B.D., AHMAD S., *Sensor. Actuat. B-Chem.*, 138 (2009), 572.
- [6] MAHDAVI M., AHMAD M., HARON M., NAMVAR F., NADI B., RAHMAN M., AMIN J., *J. Mol.*, 18 (2013), 7533.
- [7] NEMALA H., THAKUR J.S., NAIK V.M., VAISHNAVA P.P., LAWES G., NAIK R., *J. Appl. Phys.*, 116 (2014), 034309.
- [8] IWASAKI T., NAKATSUKA R., MURASE K., TAKATA H., NAKAMURA H., WATANO S., *Int. J. Mol. Sci.*, 14 (2013), 9365.
- [9] ZHANG L., HE R., GU H.C., *Appl. Surf. Sci.*, 253 (2006), 2611.
- [10] LAURENT S., FORGE D., PORT M., ROCH A., ROBIC V., ELST L.V., MULLER R.N., *Chem. Rev.*, 108 (2008), 2064.
- [11] SONG N.N., YANG H.T., LIU H.L., REN X., DING H.F., ZHANG X.Q., CHENG ZH., *Sci. Rep.-UK*, 3 (2013), 3161.
- [12] LANGFORD J.I., WILSON A.J.C., *J. Appl. Crystallogr.*, 11 (1978), 102.
- [13] CHEN Y.-J., TAO J., XIONG F., ZHU J.-B., GU N., ZHANG Y.-H., DING Y., GE L., *Drug. Dev. Ind. Pharm.*, 36 (2010), 1235.
- [14] CAIZER C., *Nanoparticle Size Effect on Some Magnetic Properties, Handbook of Nanoparticles*, Springer, Switzerland, 2016 p.475.
- [15] MORADMARD H., SHAYESHTCH S.F., TOHIDI P., ABBAS Z., KHALEGI M., *J. Alloy. Compd.*, 650 (2015), 116.
- [16] SRIVASTAVA M., SINGH J., MISHRA R.K., SINGH M.K., OJHA A.K., YASHPAL M., SUDHANSHU S., *Curr. Appl. Phys.*, 14 (2014), 980.
- [17] JOSHI S., KUMAR M., CHHOKER S., SRIVASTAVA G., JEWARIYA V., SINGH V.N., *J. Mol. Struct.*, 1076 (2014), 55.

- [18] NAIDU C.B.K., MADHURI W., *Mater. Chem. Phys.*, 181 (2016), 432.
- [19] GABAL M.A., ALANGARI Y.M., ZAKI H.M., *J. Magn. Magn. Mater.*, 363 (2014), 6.
- [20] HOSSAIN A.A., BISWAS T., YANAGIDA T., TANAKA H., TABATA H., KAWAIT., *Mater. Chem. Phys.*, 120 (2010), 461.
- [21] TKACH A., VILARINHO P.M., KHOLKIN., *J. Appl. Phys. A*, 79 (2004), 2013.
- [22] JONSCHER A.K., *Nature*, 267 (1977), 673.
- [23] MOCANU Z.V., AIRIMIOAEI M., CIOMAGA C.E., CURECHERIU L., TUDORACHE F., TASCU S., IORDAN A.R., PALAMARU N.M., MITOSERIU L., *J. Mater. Sci.*, 49 (2014), 3276.
- [24] ABDEEN A.M., *J. Magn. Magn. Mater.*, 185 (1998), 199.
- [25] MANOHAR A., KRISHNAMOORTHY C., *Mater. Chem. Phys.*, 192 (2017), 235.
- [26] NAIDU C.B.K., KIRAN R.S., MADHURI W., *Mater. Res. Bull.*, 89 (2017), 125.
- [27] BATOO K., ANSARI M., *J. Nano Res. Lett.*, 7 (2012), 112.
- [28] VERMA K., KUMAR A., VARSHNEY D., *J. Alloy. Compd.*, 526 (2012), 91.
- [29] YOUNAS M., NADEEM M., ATIF M., GROSSING R., *J. Appl. Phys.*, 109 (2011), 093704.
- [30] BEHERA B., NAYAK P., CHOUDHARY R., *J. Alloy. Compd.*, 436 (2007), 226.
- [31] MANDAL S.K., SINGH S., DEY P., ROY J.N., MANDAL P.R., NATH T.K., *J. Alloy. Compd.*, 656 (2016), 887.
- [32] OLIVEIRA DE H.P., ANDRADE C.A.S., MELO DE C.P., *J. Colloid. Interf. Sci.*, 319 (2008), 441.
- [33] CHALIKIAN T.V., *J. Phys. Chem. B*, 102 (1998), 6921.
- [34] HÖCHTL P., BORESCH S., STEINHAUSER O., *J. Chem. Phys.*, 112 (2000), 9810.
- [35] JANSSON H., BERGMAN R., SWENSON J., *J. Non-Cryst. Solids*, 351 (2005), 2858.
- [36] TAIT M.J., SUGGETT A., FRANKS F., ABLETT S., QUICKENDEN P.A., *J. Solution Chem.*, 1 (1972), 131.
- [37] FRANKS F., REID D.S., SUGGETT A., *J. Solution Chem.*, 2 (1973), 99.

Received 2017-07-19
Accepted 2017-10-30